Journal of Power Sources 273 (2015) 716–723

Contents lists available at ScienceDirect

Journal of Power Sources

journal homepage: www.elsevier.com/locate/jpowsour

Sulfur and carbon tolerance of $BaCeO_3$–$BaZrO_3$ proton-conducting materials

D. Medvedev [a], J. Lyagaeva [a], S. Plaksin [a], A. Demin [a, **], P. Tsiakaras [a, b, *]

[a] Laboratory of Electrochemical Devices Based on Solid Oxide Proton Electrolytes, Institute of High Temperature Electrochemistry, Yekaterinburg 620990, Russia
[b] Department of Mechanical Engineering, School of Engineering, University of Thessaly, Pedion Areos, Volos 383 34, Greece

HIGHLIGHTS

- BCZYx ceramic materials were obtained by citrate-nitrate combustion method.
- The stability of BCZYx against H_2O-, CO_2- and H_2S-containing atmospheres was evaluated.
- 30 mol.% of Zr in $BaCeO_3$-based system guarantees the good tolerance properties.
- BCZY0.3 exhibited acceptable conductivity in different atmospheres.

GRAPHICAL ABSTRACT

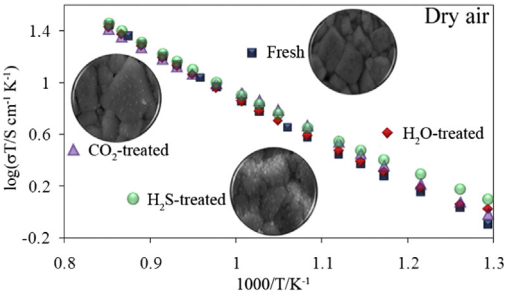

ARTICLE INFO

Article history:
Received 21 June 2014
Received in revised form
19 August 2014
Accepted 16 September 2014
Available online 26 September 2014

Keywords:
$BaCeO_3$
$BaZrO_3$
Perovskite
Proton-conducting electrolyte
Phase stability
SOFC

ABSTRACT

In the present work, $BaCe_{0.8-x}Zr_xY_{0.2}O_{3-\delta}$-based ceramic samples (BCZYx) are prepared and their chemical stability in corrosive atmospheres containing high concentrations of H_2O, CO_2 and H_2S is investigated. Based on both the fresh (not exposed) and the treated (exposed to corrosive atmospheres) samples, the estimation of the tolerance degree is obtained by determining the: i) phase structures, ii) unit cell parameters, iii) surface microstructures, and iv) electrical conductivities. Fresh ceramics is found to be single-phased in the whole range of x. It is also found that all the treated materials exhibit good chemical stability in the water vapor atmosphere, whereas the samples with $0 \le x \le 0.2$ and $0 \le x \le 0.3$ are not single-phased in pure CO_2 and 10% H_2S/Ar, respectively. The analysis of crystal structure and transport characteristics of the treated BCZY0.3 samples is shown a weak deviation of unit cell parameters and no degradation in electrical conductivity. For fresh BCZY0.3 the transport nature in various atmospheres is evaluated. At 600 °C the BCZY0.3 exhibits conductivity of 2.7, 4.0, 1.7 and 3.7 mS cm^{-1} in air, wet air, hydrogen and wet hydrogen atmospheres, respectively. Based on the obtained results, BCZY0.3 can be considered as a perspective proton-conducting material having reasonable transport and tolerance properties.

1. Introduction

High temperature proton conductors (HTPCs) constitute a unique class of oxide materials possessing both protonic as well as oxygen-ion conductivity in H_2 and H_2O containing atmospheres [1–4]. Such exceptional properties underpin the potential application of HTPCs in a wide range of solid oxide electrochemical

* Corresponding author. Tel.: +30 24210 74065; fax: +30 24210 74050.
** Corresponding author. Tel.: +7 343 3745431; fax: +7 343 3745992.
E-mail addresses: A.Demin@ihte.uran.ru (A. Demin), tsiak@mie.uth.gr (P. Tsiakaras).

http://dx.doi.org/10.1016/j.jpowsour.2014.09.116
0378-7753/

devices, such as hydrogen sensors, pumps, reactors, oxygen and hydrogen permeable membranes, electrolyzes and fuel cells [3–8].

Currently, proton conductors are being extensively used as electrolytes for solid oxide fuel cells (SOFCs). It has been theoretically predicted and experimentally confirmed that the efficiency of the SOFCs based on proton-conducting materials exceeds that of the SOFCs based on unipolar oxygen-conducting electrolytes and can amount to 80% [9].

Numerous research works have shown that a high level of protonic conductivity was achieved for $BaCeO_3$ and $BaZrO_3$ doped oxides. However, there are serious drawbacks limiting the potential use of such compounds [1,8,10]: i) the high level of grain boundary resistance as a part of total resistance prevailing for materials on the base of $BaZrO_3$, ii) the extremely high sintering temperatures required for dense ceramic's formation, and iii) the insufficient thermodynamic stability of $BaCeO_3$-based systems against H_2O, CO_2 and H_2S:

$$BaCeO_3 + H_2O \rightarrow Ba(OH)_2 + CeO_2, \quad (1)$$

$$BaCeO_3 + CO_2 \rightarrow BaCO_3 + CeO_2, \quad (2)$$

$$BaCeO_3 + H_2S \rightarrow BaS + H_2O + CeO_2. \quad (3)$$

The first two problems can simultaneously be solved by adding small amount of sintering additives to the initial precursors [11–13], whereas a significant enhance of stability of barium cerate is realized through partial substitution of host ions with elements possessing more acidic properties (for example, In^{3+}, Ti^{4+}, Nb^{5+}) [14–18]. Unfortunately, such modification of $BaCeO_3$ inevitably leads to a decrease in its ionic conductivity due to the structure changes of ABO_3 perovskites (lattice free volume decreasing or narrowing of B–O bond length) [8].

Zirconium can be considered as one of the most suitable dopants for $BaCeO_3$ systems, because Zr-introduction has a less dramatic effect on conductivity deterioration and, at the same time, a considerable enhancement of materials' thermodynamic stability [1,6,8]. Moreover, $BaCeO_3$ and $BaZrO_3$ form a wide range of solid solutions, that prevent the appearance of undesirable phase(s) in the case of high substitution level [1,8].

From these viewpoints, much research in the recent years has focused on the development of new HTPCs based on $BaCeO_3$–$BaZrO_3$ solid solutions [19–22]. However, there are considerable disagreements concerning the optimal concentration of zirconium required for acceptable stability and sufficient conductivity of mixed $BaCeO_3$–$BaZrO_3$ systems [8]. Probably, the differences in the results of stability associated with the various testing experiments (gas concentration, temperature, soaking time) and the nature and concentration of dopant or co-dopants. Mostly, the investigation of materials stability is limited by the experimental methods (X-Ray diffraction analysis or thermogravimetry) without the use of theoretical ones (for example, thermodynamic calculations). Thus, it is interesting to verify the stability of cerate-zirconate materials in various corrosive atmospheres, but at other conditions being equal (temperature and soaking time), as well as to compare these data with those obtained from the thermodynamic calculations.

The present work focuses on: i) the synthesis features of $BaCe_{0.8-x}Zr_xY_{0.2}O_{3-\delta}$ + 1 wt.% CuO or Co_3O_4 (BCZYx; $0 \le x \le 0.8$, $\Delta x = 0.1$) ceramic samples and ii) the thorough evaluation of zirconium substitution effect on their structure, phase stability properties and electrical characteristics.

2. Experimental

Among the others, the effect of zirconium content on the physical, structure and stability properties of a new proton-conducting perovskite series of $BaCe_{0.8-x}Zr_xY_{0.2}O_{3-\delta}$ + 1 wt.% MO_n (MO_n = CuO for $0 \le x \le 0.5$ or Co_3O_4 for $0.6 \le x \le 0.8$) has been investigated in the present study. The copper and cobalt oxides as sintering additives were selected on the basis of our preliminary studies from the viewpoints of both ceramics densification data (not present here) and its relatively high solubility in the perovskite structure in contrast to nickel or zinc [8]. The prepared materials were designated as BCZYx.

2.1. Powders and ceramics preparation

BCZYx samples were prepared by a modified version of citrate-nitrate combustion synthesis with subsequent decomposition of organometallic complexes at high temperatures. Prior to the synthesis, the starting materials ($Ba(NO_3)_2$, $Ce(NO_3)_3 \cdot 6H_2O$, $Y(NO_3)_3 \cdot 6H_2O$, CuO, Co_3O_4 and citric acid, with purity no less than 99.5%), were thoroughly mixed and dissolved afterward in a solution containing stoichiometric required amounts of zirconium oxynitrate and glycerin. Citric acid and glycerin were chosen as chelating and complexing agents with the appropriate molar ratio to metal nitrates (0.5:1.5:1, respectively). The as-obtained solutions were heated and stirred at 100 °C for 0.5 h with subsequent addition of ammonium hydroxide to ensure pH at the level of 8–9. The final solution was again heated at 250 °C to evaporate the excess water and assist in foaming of a viscous gel, which was eventually autoignited. The obtained gray (for low Zr content) or black (for high Zr content) powders were subsequently fired at 700 °C (1 h) in air to remove organic residue, and then the light-colored ones were calcined at 1150 °C (5 h) to form single-phase products. The powders were milled in a planetary mill (Fritsch Pulverisette 6) for 1 h at 250 rpm, uniaxially pressed into the pellets under 4 ton cm^{-2} and then sintered at 1450 °C for 5 h.

2.2. Materials characterization

The calcined powders were examined by X-ray powder diffraction analysis (XRD, D/MAX-2200 RIGAKU) using $CuK_{\alpha 1}$ radiation at room temperature in ambient air. The scans ranged between $20^\circ \le 2\theta \le 90^\circ$ with an interval of 1° min^{-1}. The identification of the materials' phase composition and crystal structure were performed according to the Joint Committee on Powder Diffraction Standards data file by employing MDI Jade 6 software. Since the material's structure changes from orthorhombic symmetry to cubic one with increasing x in BCZYx, the pseudocubic lattice parameter was used for comparison between the different samples. The pseudocubic lattice parameter was found as: $a_{pseudocubic} = (a \cdot b \cdot c/4)^{1/3}$, $a_{pseudocubic} = (a^2 c \cdot \sqrt{3}/12)^{1/3}$ and $a_{pseudocubic} = a$ for orthorhombic, rhombohedral and cubic structures, respectively. The dimensions of the sintered ceramics were measured before and after sintering to follow the shrinkage and density characteristics. In addition, the geometric density of ceramics was compared with that calculated on the base of the hydrostatic weighting method in kerosene. Both sets of data were shown to be in excellent agreement. The relative density was found to be more than 94% for BCZY0–BCZY0.6, about 88% for BCZY0.7 and 90% for BCZY0.8. The morphology of the sintered samples was investigated by scanning electron microscopy (SEM, JSM-5900 LV).

2.3. Chemical stability and electrical properties

For the evaluation of the thermodynamic stability at elevated temperatures and under H_2O, the BCZYx ceramic samples, already placed inside a quartz tube, were exposed to air (at 700 °C for 10 h), previously passed through the boiling water. In order to investigate the chemical stability of the BCZYx ceramic samples in a CO_2-containing atmosphere, the second set of samples were also placed inside a quartz tube and then exposed to pure CO_2 at 700 °C for 10 h. Furthermore, the third set of BCZYx ceramic samples were treated by H_2S (10 vol.% in Ar, 700 °C, 10 h) which is a impurity component of a fossil fuel. After H_2O, CO_2 or H_2S exposures, the phase structure of each treated sample was investigated by XRD. The conductivity of the optimal sample was investigated by a standard four probe dc-method utilizing the microprocessor system ZIRCONIA-318 at 500–900 °C at the different atmospheres (dry air, wet air, dry hydrogen and wet hydrogen) and between 10^{-20}–0.21 atm of oxygen partial pressures (pO_2) at different temperatures. Moreover, the conductivity response of the optimal sample before and after treatments was analyzed. The dry and wet conditions were created by gas pumping through calcined zeolite (the residual steam partial pressure is equal approximately 0.001 atm) and the bubbler at 25 °C (the water partial pressure is equal approximately 0.03 atm), respectively.

3. Results and discussion

3.1. Phase structure of synthesized materials

All the sintered BCZYx ceramics were identified by using XRD analysis. The obtained materials were consisted by a single-phase perovskite-type structure indicating the formation of solid solutions over the entire investigated range of x (Fig. 1). However, conflicting definitions in literature about the crystal structure of the same materials (i.e. $BaCe_{0.8-x}Zr_xY_{0.2}O_{3-\delta}$) were found. This might be because several factors are known to affect the phase equilibrium, such as the preparation methods, the temperature regimes of calcination/sintering, the concentration of uncontrolled impurities in the initial precursors, and even the moisture of ambient atmospheres. For example, Fabbri et al. [22] reported the monoclinic structure for Zr-free barium cerate ($x = 0$), whereas the cubic one was detected for $x = 0.3$, 0.5 and 0.8. The work of Guo et al. [23] showed that the lattice symmetry for the samples with $x = 0$, $0.1 \le x \le 0.5$ and $0.6 \le x \le 0.8$ can be indexed as monoclinic, orthorhombic and cubic, respectively. Sawant et al. [24] found the orthorhombic structure for $x = 0$ and the cubic one for $x \ge 0.2$. The results of *Tu* et al. [25] demonstrated the formation of the rhombohedral phase with a small impurity of the monoclinic one for $0 \le x \le 0.3$ and the pure cubic perovskite for $0.4 \le x \le 0.8$. Han et al. [26] revealed that $BaCe_{0.8}Y_{0.2}O_{3-\delta}$ ($x = 0$) is characterized by the rhombohedral and monoclinic structures at room temperature in dry and wet oxygen, respectively.

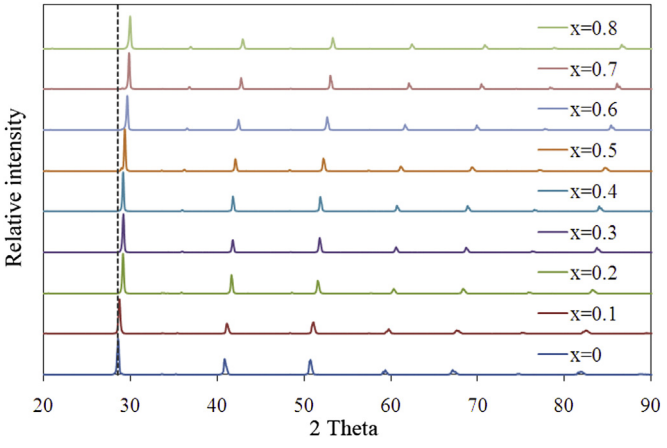

Fig. 1. XRD patterns of fresh BCZYx ceramics.

In the present work, at low concentration of zirconium (BCZY0, BCZY0.1 and BCZY0.2) the perovskite structure was found to be orthorhombic (space group Pmcn), whereas the crystal structure of BCZY0.3 was identified as a rhombohedrally distorted perovskite (space group $R\bar{3}$ C); finally, for BCZY0.4–BCZY0.8 ceramics the cubic perovskite (space group $Pm\bar{3}$ m) was realized. An increase in the crystal symmetry in a BCZYx system is closely associated with an increase in the tolerance factor (t) from 0.935 for $BaCe_{0.8}Y_{0.2}O_{3-\delta}$ to 0.987 for $BaZr_{0.8}Y_{0.2}O_{3-\delta}$ (Table 1) and a decrease in both the Ce(Zr)–O length bond and Ce(Zr)–O–Ce(Zr) octahedrons tilting [27]. Moreover, substitution of Ce^{4+} by Zr^{4+} leads to a decrease in the unit cell parameters (which were compared with each other in a pseudocubic system, Table 1) due to the size factor ($Zr^{4+}_{VI} = 0.72$ Å, $Ce^{4+}_{VI} = 0.87$ Å) [28]. This tendency can be clearly seen in Fig. 1 from the viewpoint of a slight shift of the reflection lines toward higher angles with increasing x. It is worth noting that no Cu- or Co-extra reflexes were observed on the XRD patterns showing possible dissolution of 3d-elements in the cationic sublattice of a perovskite. However, it seems that the small concentration of 3d-transition elements should not play an essential role in changing crystal parameters.

3.2. Phase stability

The Ce^{4+} by Zr^{4+} substitution in the $BaCe_{1-x}Zr_xO_3$-based systems is required in order to enhance the thermodynamic stability of the materials in the presence of salt-forming (CO_2, SO_2, H_2S) and hydroxide-forming (H_2O) gas components. The barium cerate oxides unmodified by stabilizing dopants decompose to a CeO_2 solid solution and corresponding hydroxide or salts of barium (carbonate, sulfite and sulfide).

When BCZYx ceramics were treated by H_2O at 700 °C for 10 h, no CeO_2 and $Ba(OH)_2$ impurities were found by XRD analysis performed after water exposures (this data not shown). Moreover, the perovskite phase remains chemically stable even for BCZY0, confirming the tolerance of this oxide to the conditions used. According to literature [29,30], at temperature values higher than 400 °C the stability of $BaCeO_3$-based ceramics is satisfactory, whereas for low temperature range the perovskite materials fully or partially decompose, particularly in boiling water [18,31,32].

The chemical nature of BCZYx significantly changes in CO_2-containing gas atmospheres. The reaction between ceramic samples and CO_2 is registered by XRD analysis for low value of x,

Table 1
Crystal parameters of fresh BCZYx sintered at 1450 °C for 5 h.

x	Space group	Unit cell parameters			$V_{pseudocubic}$ (Å^3)	t
		a (Å)	b (Å)	c (Å)		
0	Pmcn	8.7667	6.2427	6.2317	85.26	0.935
0.1	Pmcn	8.7235	6.2078	6.1878	83.77	0.941
0.2	Pmcn	8.6821	6.1705	6.1523	82.40	0.948
0.3	$R\bar{3}$ C	6.1440		15.0061	81.76	0.954
0.4	$Pm\bar{3}$ m	4.3018			79.61	0.960
0.5	$Pm\bar{3}$ m	4.2854			78.70	0.967
0.6	$Pm\bar{3}$ m	4.2531			76.93	0.974
0.7	$Pm\bar{3}$ m	4.2249			75.41	0.980
0.8	$Pm\bar{3}$ m	4.2052			74.36	0.987

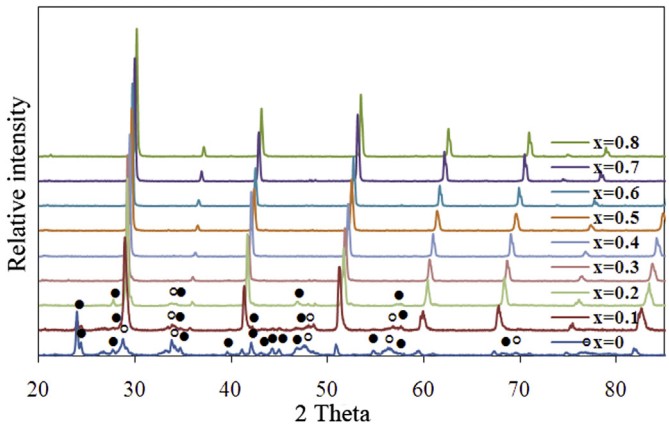

Fig. 2. XRD patterns of treated BCZYx ceramics after CO_2 exposure at 700 °C for 10 h. Key: ○ – CeO_2-like phase, ● – $BaCO_3$.

whereas other materials are stable (Fig. 2). It is commonly known that the introduction of Zr^{4+} improves the thermodynamic stability of $BaCeO_3$-based materials due to the reduction of the M–O bond strength, with a corresponding change of the oxide properties from basic to acidic [8]. At the same time, the tolerance factor (Table 1) can also cause an increase in the materials stability. Our results are in an excellent agreement with the literature data (see work [33] and Table 13 in Ref. [8]), which show that the chemical interactions on the XRD patterns are suppressed just at x not less than 30 mol.% in B-position of ABO_3 perovskite because no formation of $BaCO_3$ and CeO_2 solid solution was observed for these samples.

Finally, the phase stability of BCZYx was also studied under H_2S-treatment (Fig. 3). The significant interaction between the Ce-rich materials is observed to result in the formation of oxide, sulfide and oxysulfide compounds. The XRD data demonstrates that the intensity of impurity reflexes decreases with a gradual growth of x and is insignificant for $x \geq 0.4$. In addition, the sulfidation was visually observed, because the dense ceramic samples with $x = 0$ and 0.1 crumbled to the powders during the high temperature H_2S-exposure (as opposed to H_2O- and CO_2-exposures), whereas the materials retain their integrity at higher zirconium concentrations. This fact indicates that the sulfidation front is not limited by the surface and penetrates into the ceramics volume with the formation of the S-containing phases, which cause the samples destruction. It should be noted that the XRD pattern of treated BCZY0.2 illustrates the formation of perovskite structure with an

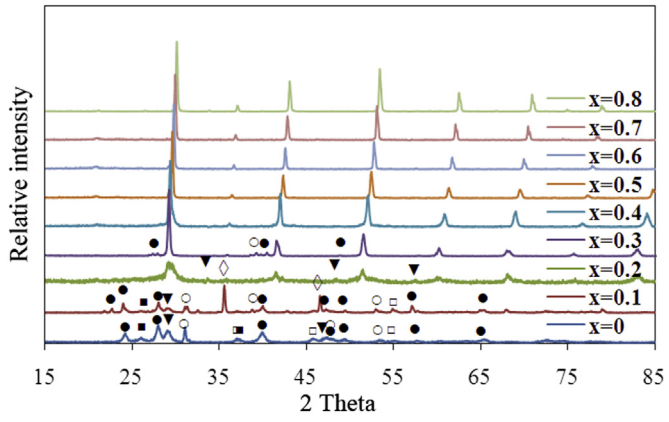

Fig. 3. XRD patterns of treated BCZYx ceramics after 10% H_2S/Ar exposure at 700 °C for 10 h. Key: ● – BaS, ○ – Y_2O_2S, ■ – Ce_2O_2S, ▼ – CeO_2-like phase, ◊ – unidentified phase(s).

impurity phase on the base of CeO_2; therewith peak broadening indicates on the amorphization of this sample. Therefore, H_2S must be considered as a more aggressive component for BCZYx than H_2O and CO_2.

As shown in Fig. 3, the chemical interaction between the $BaCeO_3$–$BaZrO_3$-based perovskites and H_2S has a more complicated character than in the case of H_2O- and CO_2-treatments. The decomposition of Ce-rich BCZYx samples is followed by the formation of both barium sulfide, a (Ce, Zr)O_2-like phase:

$$BaCe_{0.8-x}Zr_xY_{0.2}O_{3-\delta} + H_2S \rightarrow BaS + Ce_{0.8-x}Zr_xY_{0.2}O_{3-\delta}, \quad (4)$$

and cerium and yttrium oxysulfides, as schematically shown below:

$$2CeO_2 + H_2S \xrightarrow{[H]} Ce_2O_2S + H_2O, \quad (5)$$

$$Y_2O_3 + H_2S \rightarrow Y_2O_2S + H_2O. \quad (6)$$

To estimate the effect of different treatments on the crystal structure of stable BCZY0.3–BCZY0.8 materials, the XRD analysis of H_2O-, CO_2- and H_2S-treated samples is carried out. In Fig. 4 one can notice the slightly distinguishable changes in the cubic cell parameter of the treated samples in comparison with the fresh ones. The maximal deviation of the unit cell parameters, obtained before and after the stability experiments, is equal to about 0.22% for the BCZY0.8 sample.

Although, the XRD data shows that the CO_2-treatment results in the maintenance of a single-phase material for BCZY0.3, from the SEM micrographs (Fig. 5b) no any visible change in the grain boundary microstructure (respectively the basic sample, Fig. 5a) can be seen; however, small amounts of impurity phase(s) with size of 100–400 nm localized at the grain surface can be distinguished. Electron microprobe analysis confirms the increased carbon concentration in the nanoscale sediments. A significant change in the microstructure of BCZY0.3 ceramic after H_2S-treatment (Fig. 5c) was observed, because of the presence of additional impurity reflexes with low intensity on the XRD pattern. The size of these sediments is the same as in the previous case; however their number is considerably higher. Thereby, according to the XRD data coupled with SEM results, the stability range of BCZYx system is equal $0.3 \leq x \leq 0.8$ in the case of CO_2 exposure and narrows to $0.4 \leq x \leq 0.8$ in the case of high H_2S concentration. Considering that the concentration of hydrogen sulfide in fossil fuels is at the level of some ppm, we can assume that the sample with $x = 0.3$ also has an acceptable phase stability at lower H_2S-concentration. This assumption is confirmed by other investigations. For example, Yang

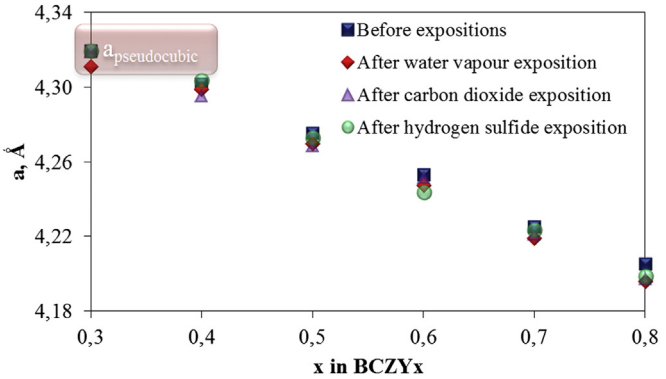

Fig. 4. The concentration dependences of cubic unit cell parameters of fresh and treated BCZYx ceramics.

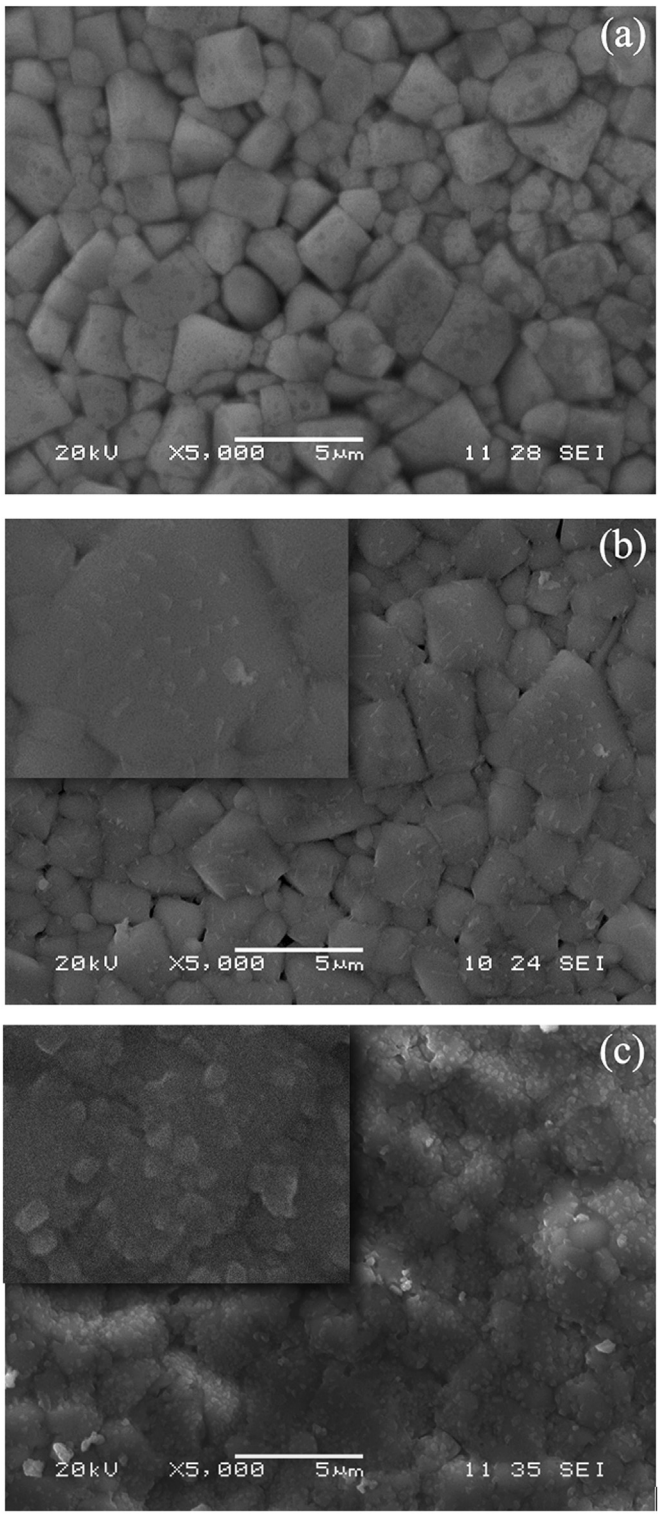

Fig. 5. The microstructure of fresh (a), CO_2-treated (b) and H_2S-treated (c) BCZY0.3 ceramics.

et al. stated the excellent stability of $BaCe_{0.7}Zr_{0.1}Y_{0.1}Yb_{0.1}O_{3-\delta}$ electrolyte to sulfur poisoning (20–50 ppm of H_2S) even for lower zirconium concentration in $BaCeO_3$ [34].

For understanding of the fact of impurity phase formation, the thermodynamic calculations were carried out for the reactions (1)–(3) in the case of simplified oxides ($BaCe_{1-x}Zr_xO_3$, where $x = 0$, 0.3 and 1). The standard Gibbs free energy change (ΔG_T^o) was computed on the base of the thermodynamic properties of parties of reactions (Table 2) [35–37]. The Gibbs free energy change (ΔG_T) was found as follows:

Table 2
Thermodynamic properties of the substances.

Substance	$\Delta_f H^0$(kJ mol^{-1})	S^0 (J mol^{-1} K^{-1})	Ref.
$BaCeO_{3(s)}$	−1690.0	144.5	[35]
$BaZrO_{3(s)}$	−1775.6	124.62	[36]
$H_2O_{(g)}$	−241.9	188.8	[37]
$CO_{2(g)}$	−393.51	213.79	[37]
$H_2S_{(g)}$	−20.6	205.8	[37]
$CeO_{2(s)}$	−1089.4	62.3	[37]
$ZrO_{2(s)}$	−1100.6	50.36	[37]
$Ba(OH)_{2(s)}$	−944.7	107.0	[37]
$BaCO_{3(s)}$	−1213.0	112.1	[37]
$BaS_{(s)}$	−460.0	78.2	[37]

$$\Delta G_{T,(1-3)} = \Delta G^o_{T,(1-3)} + RTlnK_{1-3}, \quad (7)$$

where R is the universal gas constant, T is the absolute temperature, K_{1-3} are the equilibrium constants of reactions (1)–(3). For the calculations, the following assumptions were taken into account: i) $pH_2O = pCO_2 = 1$ atm, $pH_2S = 0.1$ atm; ii) the Gibbs free energy change for cerate-zirconate oxide was equal the partial sum of ones for $BaCeO_3$ and $BaZrO_3$; iii) in the case of eq. (3) water forms in the right part of the reaction, the equilibrium partial pressure of which was assumed approximately close to 0.01 atm.

Fig. 6 shows the temperature dependences of Gibbs free energy change corresponding to hydration, carbonization and sulfidation processes of $BaCeO_3$, $BaZrO_3$ and mixed cerate-zirconate oxide.

As mentioned above, the thermodynamic stability of investigated perovskite materials against H_2O can be considered as satisfactory in the intermediate- and high-temperature ranges due to the positive value of$\Delta G_{T,1}$. Indeed, the formation of barium hydroxide and CeO_2-like phase is thermodynamically possible just at temperatures not more than 400 °C (Fig. 6a). The experimental data of Haile et al. [29], Wu et al. [30] and Matsumoto et al. [38] confirm these theoretical computations.

The Gibbs free energy change of carbonization ($\Delta G_{T,2}$) riches the positive values at ~950, 800 and 550 °C in the case of $x = 0$, 0.3 and 1, respectively, and grow with following increasing temperature (Fig. 6b). Thereby, theoretical calculations do not ban the possibility of formation of secondary phases in BCZY0.3 sample at 700 °C. However, the good phase and microstructure stability of this material, probably, is the cause of the kinetic difficulties or structure features. Indeed, there are data showing the tolerance properties of $BaCeO_3$–$BaZrO_3$ ceramic samples against CO_2 even for lower concentration of zirconium. For example, in above mentioned work of Yang et al. [34] $BaCe_{0.7}Zr_{0.1}Y_{0.1}Yb_{0.1}O_{3-\delta}$ material with 10 mol.% of Zr is stable in 50 vol.%H_2 + 50 vol.% CO_2 atmosphere at 750 °C during a very long period of time (300 h); Okiba et al. [39] pointed the maintenance of $BaCe_{0.9-x}Zr_xY_{0.1}O_{3-\delta}$ perovskites after treatment in pure CO_2 (900 °C, 3 h) at content of zirconium not less than 20 mol.%; the study of Lee et al. [40] shows that in the $Ba_{0.6}Sr_{0.4}Ce_{0.8-x}Zr_xY_{0.1}O_{3-\delta}$ system the materials are characterized by enhanced stability in pure CO_2 (600 °C, 12 h) in the range of $0.2 \leq x \leq 0.8$. Such results can be attributed to the fact that the perovskite decomposition and impurity phase formation are controlled by kinetic factors rather than thermodynamic ones.

Experimentally the latter statement was confirmed by Okiba et al. [39]. More precisely, they have investigated the stability of $BaCe_{0.9-x}Zr_xY_{0.1}O_{3-\delta}$ materials in the viewpoint of kinetic aspects. The authors found that the increase in zirconium content from 0 to 20 mol.% promotes the increase in kinetic stability due to the

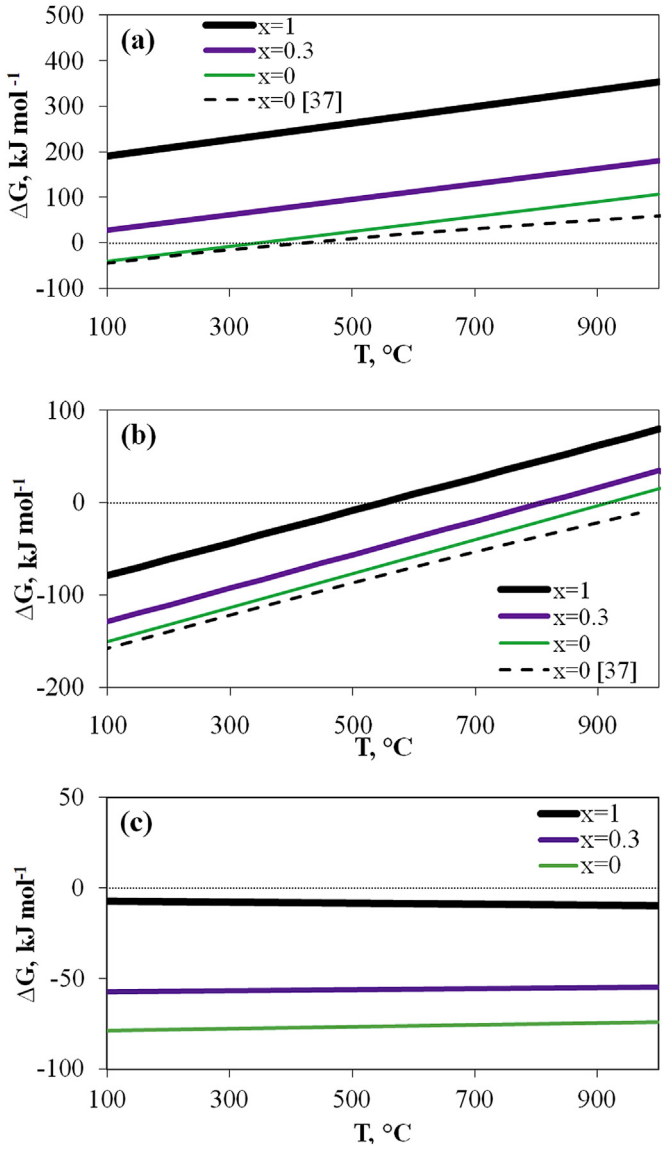

Fig. 6. Temperature dependences of Gibbs free energy change of reaction of $BaCe_{1-x}Zr_xO_3$ with H_2O (a), CO_2 (b) and H_2S (c). The thermodynamic calculations between $BaCeO_3$ and H_2O (dotted line 1) or CO_2 (dotted line 2) were performed by Matsumoto et al. [38] and presented for comparison.

decrease in apparent rate constant of carbonization reaction by order of magnitude. Guo et al. [23] using BET analysis revealed that after CO_2-treatment of the $BaCe_{0.8-x}Zr_xY_{0.2}O_{3-\delta}$ powders (650 °C, 2 h) the carbonate formation rate also decreases by order of magnitude (from $7.50\cdot10^{-6}$ to $0.87\cdot10^{-6}$ mol m^{-2} min^{-1}) with increase of x from 0 to 0.4 and by two orders of magnitude with transition from cerate to zirconate.

Moreover, there is another reason, explaining the inconsistency between theoretical and experimental data. As was noted in part 3.1, in the $BaCe_{0.8-x}Zr_xY_{0.2}O_{3-\delta}$ system the materials with a particular value of zirconium concentration can be indexed in different structures, which are function of many controlled and uncontrolled factors. Perovskite structures with higher symmetry are characterized by better stability than low symmetry structures, which follows from the concept of Goldschmidt tolerance factor. Therefore, in the work of Fabbri et al. [22] and Guo et al. [23] the stability of BCZYx materials is achieved at high x values, because of the fact that these materials have the cubic structures. In contrast, according to data of Sawant et al. [24] and Lee et al. [40], the cubic perovskite syngony in $BaCe_{0.8-x}Zr_xY_{0.2}O_{3-\delta}$ and $Ba_{0.6}Sr_{0.4}Ce_{0.8-x}Zr_xY_{0.1}O_{3-\delta}$ systems is achieved at $x \geq 0.2$ that results in their acceptable stability, despite the thermodynamic predictions.

In the case of H_2S treatment the values of $\Delta G_{T,3}$ are negative irrespective of materials composition (Fig. 6c) and weekly dependent on temperature for account of entropy factor. However the Gibbs free energy change of reaction (3) tends to null with increasing zirconium content. Therefore, the phase stability of BCZYx materials after H_2S exposure must be significantly increased with increasing x. It should be noted that our results of calculations are in a good agreement with those reported in literature [41–43], which demonstrate a rather simple formation of the impurity phases for the $BaCeO_3$-based systems and tolerant properties of the Zr-substituted barium cerate materials, as well as the possibility of oxysulfide formation under treatment of Ce-containing materials in H_2S atmosphere. At the same time, concerning the stability of zirconates or Zr-substituted cerates, the thermodynamic calculations are not in agreement with results obtained by using of XRD and/or TG methods. Despite the negative value of $\Delta G_{T,3}$, these materials practically are rather stable, as show our experiment and data reported in literature [34,41,44,45]. This "contradiction" can be explained on the basis of kinetic aspects or structure features, as above mentioned.

3.3. Electrical conductivity

Results in a several number of investigations have demonstrated that both acceptable electrical conductivity and reasonable phase stability can be achieved for cerate-zirconate ceramic materials at close concentration of cerium and zirconium [1,6–8]. From this viewpoint, the BCZY0.3 sample was chosen in the present investigation for electrical characterization.

Before direct conductivity measurements of selected sample, we investigated its electrical response in dry air atmosphere to the exposures used (Fig. 7). As it can be seen, the electrical conductivity of BCZY0.3 exhibits a similar behavior with the tendency observed in Fig. 4. The weak deviations of the conductivity values of the treated samples in the high-temperature region, in comparison with the fresh one, indicate that no considerable changes of ceramic volume (and conductivity connected with it) were occurred after 10 h of exposure; regardless the presence of impurity phases determined by XRD and SEM methods after CO_2 and H_2S treatments. However, the slight increase in conductivity of treated BCZY0.3 sample was unexpectedly observed in the case of low temperature interval. The reasons resulting in such fact remain unclear yet.

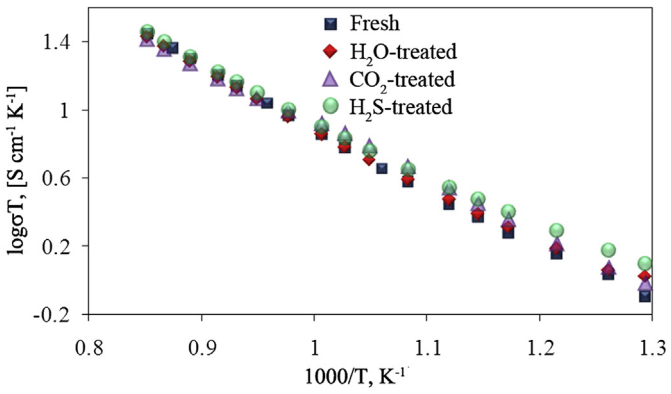

Fig. 7. The conductivity of fresh and treated BCZY0.3 ceramic samples in dry air atmosphere.

In Fig. 8a the effect of temperature on the electrical conductivity of fresh BCZY0.3 ceramic is different. Firstly, it should be noted that in the high temperature interval the conductivity of the sample is higher in oxidizing atmosphere than that in reducing one. These differences can be explained by pO_2 influence because of the mixed ionic-hole conductivity at the high oxygen partial pressure range and purely ionic transport at the low oxygen partial pressure range. The data of Fig. 8b clearly illustrates such behavior. The differences between air and hydrogen atmospheres increase as the temperature increases due to the corresponding increase of the hole contribution of total conductivity. Secondly, the steam partial pressure also strongly affects the ceramic conductivity, because of the change in protonic and oxygen-ionic contributions of total conductivity according to the well-known equation of proton defects formation ($H_2O + O_O^x + V_O^{\bullet\bullet} \Leftrightarrow 2OH_O^{\bullet}$). In the case of dry atmospheres the ionic transport of materials is determined by the moving oxygen vacancies, whereas in the steam presence the protonic transport becomes the dominant part of total conductivity, particularly for low temperature range.

In order to confirm the above mentioned conclusions, for each case the apparent activation energy (E_a) in the logσT vs. 1000/T coordinates was calculated. As it can be distinguished in Fig. 8a, in the investigated temperature range the obtained dependences are non-linear. For this reason the Ea calculation was carried out for both low- (500–700 °C) and high- (700–900 °C) temperature intervals.

It is clearly seen that in the case of air atmosphere the E_a value is lower for the wet condition than that for the dry one. This is directly related with the formation of proton defects and, correspondingly, the occurrence of proton conductivity, for which apparent activation energy is usually lower than for oxygen-ionic conductivity [46,47]. Moreover the absolute value of E_a increases with a transition from the low temperature interval to high temperature one. This tendency can be explained by prevalent contribution of the hole conductivity in the oxidizing atmosphere when temperature increases, because of the E_a for hole conductivity as a rule is higher than that for oxygen-ionic one [46–49].

As it can also be seen in Fig. 8a, the E_a values of total conductivity are significantly lower in the reducing atmospheres compared with those in the oxidizing ones, because no electronic conductivity (n- or p-type) was observed for dry or wet hydrogen [50,51].

In the case of reducing atmosphere, E_a values are again lower in the presence of water vapor and increase with increasing temperature. As is well-known the transport nature of such protonic electrolytes in the reducing conditions is determined both oxygen-ionic and protonic conductivities. At the same time, the contribution of protonic one decreases with temperature growth (see for example [46,52,53]) because of the exothermic nature of the proton defects formation reaction [1,3,4].

In Table 3 are reported the conductivity values of BCZY0.3 in comparison with the data of related cerate-zirconate ceramics, contained 30 mol.% of Zr in the Ce-position of $BaCeO_3$ perovskite. It can be seen that our results are relatively lower than that for $BaCe_{0.5}Zr_{0.3}Y_{0.2}O_{3-\delta}$ and $BaCe_{0.6}Zr_{0.3}Y_{0.1}O_{3-\delta}$, however, higher in respect to Sm-, Nd- and Er-doped analogs. Moreover, the listed data confirms the enhanced transport of proton-conducting materials in the wet conditions regardless the type of atmosphere.

The enhanced tolerance properties and comparison of conductivity values of fresh BCZY0.3 ceramic sample with literature data concerning $BaCeO_3$–$BaZrO_3$ systems allows us to consider this material as a perspective protonic (co-ionic) electrolyte for SOFC applications, which besides can be formed in the dense ceramic at relatively low sintering temperature.

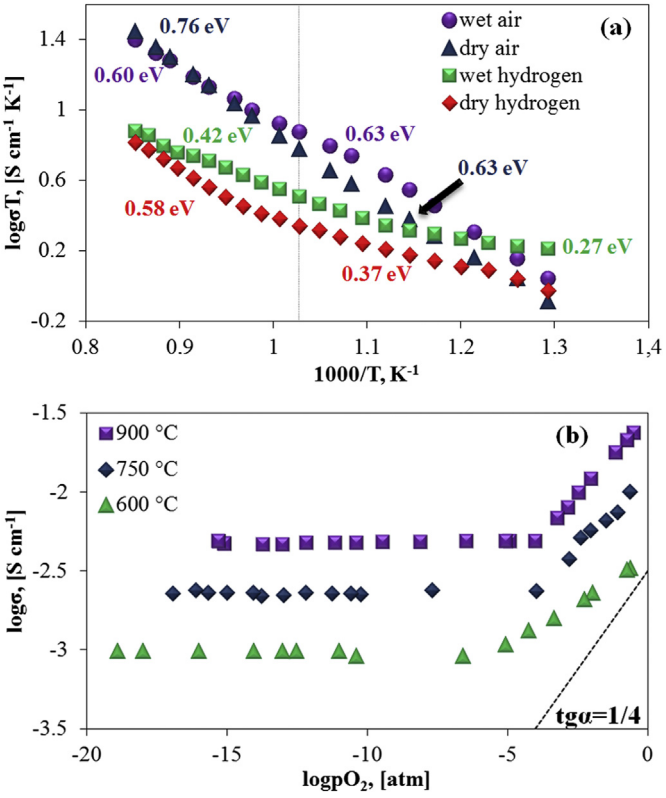

Fig. 8. The conductivity of fresh BCZY0.3 ceramic sample as a function of temperature in different atmospheres (a) and oxygen partial pressure at different temperatures (b).

4. Conclusion

The single-phase ceramic samples of $BaCe_{0.8-x}Zr_xY_{0.2}O_{3-\delta}$ + 1 wt.% CuO or Co_3O_4 (BCZYx) were obtained by the modified citrate-nitrate synthesis method. The Zr effect and type of treatment (H_2O, CO_2 and H_2S/Ar at 700 °C for 10 h) on the phase structure, unit cell parameters and microstructure were investigated. Fresh ceramics is found to be single-phased in the whole range of *x*. However, BCZYx materials exhibited a different perovskite structure with the orthorhombic, rhombohedral and cubic syngony for $0 \le x \le 0.2$, $x = 0.3$ and $0.4 \le x \le 0.8$, respectively.

Table 3
The conductivity value of fresh BCZY0.3 and related materials contained 30 mol.% of Zr in the Ce-position of perovskite $BaCeO_3$ at 600 °C.

Material	Conditions	σ (mS cm^{-1})	Ref.
$BaCe_{0.5}Zr_{0.3}Y_{0.2}O_{3-\delta}$ + 1 wt.% CuO	Dry air	2.7	This work
	Wet air	4.0	
	Dry H_2	1.7	
	Wet H_2	3.8	
$BaCe_{0.6}Zr_{0.3}Y_{0.1}O_{3-\delta}$	Wet air	7.4	[11]
$BaCe_{0.6}Zr_{0.3}Y_{0.1}O_{3-\delta}$ + 4 mol.% ZnO	Wet air	6.9	
$BaCe_{0.55}Zr_{0.3}Sm_{0.15}O_{3-\delta}$	Air	1.6	[19]
	Wet H_2	3.0	
$BaCe_{0.5}Zr_{0.3}Y_{0.2}O_{3-\delta}$	Air	4.6	[22]
	Wet H_2	7.8	
$BaCe_{0.6}Zr_{0.3}Nd_{0.1}O_{3-\delta}$	Dry H_2	2.4	[23]
$BaCe_{0.5}Zr_{0.3}Y_{0.2}O_{3-\delta}$	Wet H_2	8.6	[33]
$BaCe_{0.5}Zr_{0.3}Gd_{0.15}Pr_{0.05}O_{3-\delta}$	Air	1.5	[45]
	Wet H_2	6.9	
$BaCe_{0.6}Zr_{0.3}Nd_{0.1}O_{3-\delta}$	Air	1.6	[54]
$BaCe_{0.55}Zr_{0.3}Er_{0.15}O_{3-\delta}$	Wet H_2	0.9	[55]
$BaCe_{0.6}Zr_{0.3}Y_{0.1}O_{3-\delta}$	Wet air	7.1	[56]
	Wet H_2	8.8	
$BaCe_{0.5}Zr_{0.3}Y_{0.2}O_{3-\delta}$ + 4 mol.% ZnO	Wet H_2	5.0	[57]

The decomposition of BCZYx was observed at $x \leq 0.2$ when treated with CO_2 and H_2S; however no degradation was noted in the case of water vapor exposure. For the ceramic sample with $x = 0.3$ (BCZY0.3) the perovskite structure was maintained in the case of CO_2- and H_2S-exposures with the formation of small amount of impurity phases. A high density with close-packed and well-developed grains is achieved for BCZY0.3 ceramic. At the same time, for CO_2- and H_2S-treaded BCZY0.3 samples nanostructure impurity sediments localized on grain surface are observed. The analysis of crystal structure and transport characteristics of the treated BCZY0.3 samples showed a weak deviation of the unit cell parameters and no degradation in electrical conductivity.

The thermodynamic calculation of hydration, carbonization and sulfidation processes demonstrated that with x increasing in $BaCe_{1-x}Zr_xO_3$ system the stability of materials significantly increases against H_2O, CO_2 and H_2S. In the case of H_2O treatment, the Gibbs free energy change values of reaction between barium cerate and water vapor are positive at temperatures higher than 400 °C. Under CO_2 exposure, the carbonization of $BaCeO_3$ suppress just at temperatures not lower than 950 °C, whereas $BaZrO_3$ is stable at wide range of working temperatures (550–1000 °C). Hydrogen sulfide theoretically has a dramatically effect because of negative value of Gibbs free energy change for both $BaCeO_3$ and $BaZrO_3$ oxides between 20 and 1000 °C. However, practically zirconate and Zr-substituted $BaCeO_3$ materials are considered as rather stable. The analysis of literature results allows us to identify the reasons of significant differences in the data concerning thermodynamic stability of $BaCeO_3$–$BaZrO_3$-based materials and firstly propose possible explanations, including kinetic or structure features.

The electrical conductivity of fresh BCZY0.3 was found to be increased with the growth of both the water vapor partial pressure due to increase of proton conductivity and the oxygen partial pressure due to increase of hole conductivity. For example, the fresh BCZY0.3 exhibits conductivity of 2.7, 4.0, 1.7 and 3.8 mS cm^{-1} at 600 °C in dry air, wet air, hydrogen and wet hydrogen atmospheres, respectively. The analysis of energy activation values of electrical conductivity confirms the ionic character of transport properties in reducing atmospheres and the mixed ionic-electronic one in oxidizing conditions.

On the basis of phase stability results, transport characteristics compared with literature data, it can be considered such BCZY0.3 material as a perspective electrolyte for SOFC applications.

Acknowledgments

The authors of the present investigation are grateful to The Ministry of Education and Science of the Russian Federation (contract №. 14.Z50.31.0001) and the Research Program of the Presidium of RAS (project № 12-П-23-2006) for financial support.

The characterizations of powder and ceramic materials were carried out at the Shared Access Center “Composition of Compounds” of the Institute of High Temperature Electrochemistry. Special thanks to E.V. Kosheleva for carrying out the H_2S treatment of the samples.

References

[1] K.D. Kreuer, Annu. Rev. Mater. Res. 33 (2003) 333–359.
[2] H.J. Park, C. Kwak, K.H. Lee, S.M. Lee, E.S. Lee, J. Eur. Ceram. Soc. 29 (12) (2009) 2429–2437.
[3] K.-D. Kreuer, S.J. Paddison, E. Spohr, M. Schuster, Chem. Rev. 104 (10) (2004) 4637–4678.
[4] T. Norby, M. Widerøe, R. Glöcknera, Y. Larring, Dalton Trans. (19) (2004) 3012–3018.
[5] I.A. Amar, R. Lan, C.T.G. Petit, S. Tao, J. Solid State Electrochem. 15 (9) (2011) 1845–1860.
[6] E. Fabbri, D. Pergolesia, E. Traversa, Chem. Soc. Rev. 39 (2010) 4355–4369.
[7] E.C. Camilo de Souza, R. Muccillo, Mater. Res. 13 (3) (2010) 385–394.
[8] D. Medvedev, A. Murashkina, E. Pikalova, A. Demin, A. Podias, P. Tsiakaras, Prog. Mater. Sci. 60 (2014) 72–129.
[9] A. Demin, P. Tsiakaras, E. Gorbova, S. Hramova, J. Power Sources 131 (1–2) (2004) 231–236.
[10] E. Fabbri, L. Bi, D. Pergolesi, E. Traversa, Adv. Mater. 24 (2) (2012) 195–208.
[11] M. Amsif, D. Marrero-López, J.C. Ruiz-Morales, S.N. Savvin, P. Núñez, J. Eur. Ceram. Soc. 34 (6) (2014) 1553–1562.
[12] S. Nikodemski, J. Tong, Ryan O'Hayre, Solid State Ionics 253 (2013) 201–210.
[13] M. Ananyev, D. Medvedev, A. Gavrilyuk, S. Mitri, A. Demin, V. Malkov, P. Tsiakaras, Electrochim. Acta 125 (2014) 371–379.
[14] X. Chi, J. Zhang, Z. Wen, Y. Liu, M. Wu, X. Wu, J. Alloys Compd. 554 (2013) 378–384.
[15] K. Xie, R. Yan, X. Chen, D. Dong, S. Wang, X. Liu, G. Meng, J. Alloys Compd. 472 (1–2) (2009) 551–555.
[16] R. Yan, Q. Wang, K. Xie, Ionics 15 (4) (2009) 501–505.
[17] M. Talimi, V. Thangadurai, Ionics 17 (3) (2011) 195–200.
[18] X.-M. Liu, Y.-J. Gu, Z.-G. Liu, J.-H. Ouyang, F.-Y.Y. Yan, J. Xiang, Bull. Mater. Sci. 36 (3) (2013) 395–401.
[19] R. Kannan, S. Gill, N. Maffei, V. Thangadurai, J. Electrochem. Soc. 160 (1) (2013) F18–F26.
[20] S.J. Zhan, X.F. Zhu, W.P. Wang, W.S. Yang, Adv. Mater. Res. 554–556 (2012) 404–407.
[21] S. Ricote, N. Bonanos, A. Manerbino, W.G. Coors, Int. J. Hydrogen Energy 37 (9) (2012) 7954–7961.
[22] E. Fabbri, A. D'Epifanio, E. Di Bartolomeo, S. Licoccia, E. Traversa, Solid State Ionics 179 (15–16) (2008) 558–564.
[23] Y. Guo, Y. Lin, R. Ran, Z. Shao, J. Power Sources 193 (2) (2009) 400–407.
[24] P. Sawant, S. Varma, B.N. Wani, S.R. Bharadwaj, Int. J. Hydrogen Energy 37 (4) (2012) 3848–3856.
[25] C.-S. Tu, R.R. Chien, V.H. Schmidt, S.C. Lee, C.-C. Huang, J. Phys. Condens. Matter 24 (15) (2012) 155403.
[26] D. Han, M. Majima, T. Uda, J. Solid State Chem. 205 (2013) 122–128.
[27] W. Zając, E. Hanc, A. Gorzkowska-Sobas, K. Świerczek, J. Molenda, Solid State Ionics 225 (2012) 297–303.
[28] R.D. Shannon, Acta Crystallogr. A32 (1976) 751–767.
[29] S.M. Haile, G. Staneff, K.H. Ryu, J. Mater. Sci. 36 (5) (2001) 1149–1160.
[30] Z. Wu, M. Liu, J. Electrochem. Soc. 114 (6) (1997) 2170–2175.
[31] F. Chen, O.T.t Sørensen, G. Meng, D. Peng, J. Mater. Chem. 7 (3) (1997) 481–485.
[32] Z. Tao, Z. Zhu, H. Wang, W. Liu, J. Power Sources 195 (11) (2010) 3481–3484.
[33] Z. Shi, W. Sun, W. Liu, J. Power Sources 245 (2014) 953–957.
[34] L. Yang, S. Wang, K. Blinn, M. Liu, Z. Liu, Z. Cheng, M. Liu, Science 326 (5949) (2009) 126–129.
[35] E.H.P. Cordfunke, A.S. Booij, M.E. Huntelaar, J. Chem. Termodyn. 30 (1998) 437–447.
[36] W.-P. Gong, T.-F. Chen, Z.-P. Jin, Trans. Nonferrous Met. Soc. China 17 (2007) 232–237.
[37] J.G. Speight, Lange's Handbook of Chemistry, sixteenth ed., CD&W Inc., Laramie, Wyoming, 2005, pp. 1.237–1.279.
[38] H. Matsumoto, Y. Kawasaki, N. Ito, M. Enoki, T. Ishihara, Electrochem. Solid-State Lett. 10 (4) (2007) B77–B80.
[39] T. Okiba, F. Fujishiro, T. Hashimoto, J. Therm. Anal. Calorim. 113 (3) (2013) 1269–1274.
[40] S.-W. Lee, C.-J. Tseng, J.-K. Chang, K.-R. Lee, C.-T. Chen, I.-M. Hung, S.-L. Lee, J.-C. Lin, J. Alloys Compd. 586 (1) (2014) S506–S510.
[41] J. Li, J.-L. Luo, K.T. Chuang, A.R. Sanger, Electrochim. Acta 53 (10) (2008) 3701–3707.
[42] S. Fang, L. Bi, X. Wu, H. Gao, C. Chen, W. Liu, J. Power Sources 183 (2008) 126–132.
[43] P. Lohsoontorn, D.J.L. Brett, N.P. Brandon, J. Power Sources 175 (2008) 60–67.
[44] W.-Y. Tan, Q. Zhong, M.-S. Miao, H.-X. Qu, Ionics 15 (3) (2009) 385–388.
[45] S. Gill, R. Kannan, N. Maffei, V. Thangadurai, RSC Adv. 3 (11) (2013) 3599–3605.
[46] D.-K. Lim, C.-J. Park, M.-B. Choi, C.-N. Park, S.-J. Song, Int. J. Hydrogen Energy 35 (19) (2010) 10624–10629.
[47] S.C. Hwang, G.M. Choi, Solid State Ionics 179 (21–26) (2008) 1042–1045.
[48] Z. Shi, W. Sun, Z. Wang, J. Qian, W. Liu, ACS Appl. Mater. Interfaces 6 (7) (2014) 5175–5182.
[49] X. Chi, J. Zhang, Z. Wen, Y. Liu, J. Am. Ceram. Soc. 97 (4) (2014) 1103–1109.
[50] V.B. Balakireva, A.V. Kuz'min, V.P. Gorelov, Russ. J. Electrochem 46 (7) (2010) 749–753.
[51] N.V. Sharova, V.P. Gorelov, V.B. Balakireva, Russ. J. Electrochem. 41 (6) (2005) 665–670.
[52] S.-J. Song, E.D. Wachsman, S.E. Dorris, U. Balachandran, J. Electrochem. Soc. 150 (6) (2003) A790–A795.
[53] N.V. Sharova, V.P. Gorelov, Russ. J. Electrochem. 41 (9) (2005) 1001–1007.
[54] S. Wienströer, H.-D. Wiemhöfer, Solid State Ionics 101–103 (2) (1997) 1113–1117.
[55] J. Yin, X. Wang, J. Xu, H. Wang, F. Zhang, G. Ma, Solid State Ionics 185 (1) (2011) 6–10.
[56] K. Katahira, Y. Kohchi, T. Shimura, H. Iwahara, Solid State Ionics 138 (1–2) (2000) 91–98.
[57] Y. Li, R. Guo, C. Wang, Y. Liu, Z. Shao, J. An, C. Liu, Electrochim. Acta 95 (2013) 95–101.